nature genetics

ISPD loss-of-function mutations disrupt dystroglycan O-mannosylation and cause Walker-Warburg syndrome

Tobias Willer[1–4], Hane Lee[5,6], Mark Lommel[7], Takako Yoshida-Moriguchi[1–4], Daniel Beltran Valero de Bernabe[1–4], David Venzke[1–4], Sebahattin Cirak[8], Harry Schachter[9], Jiri Vajsar[10], Thomas Voit[11], Francesco Muntoni[8], Andrea S Loder[12], William B Dobyns[13], Thomas L Winder[14], Sabine Strahl[7], Katherine D Mathews[2,15], Stanley F Nelson[5,6], Steven A Moore[16] & Kevin P Campbell[1–4]

Walker-Warburg syndrome (WWS) is clinically defined as congenital muscular dystrophy that is accompanied by a variety of brain and eye malformations. It represents the most severe clinical phenotype in a spectrum of diseases associated with abnormal post-translational processing of α-dystroglycan that share a defect in laminin-binding glycan synthesis[1]. Although mutations in six genes have been identified as causes of WWS, only half of all individuals with the disease can currently be diagnosed on this basis[2].
A cell fusion complementation assay in fibroblasts from undiagnosed individuals with WWS was used to identify five new complementation groups. Further evaluation of one group by linkage analysis and targeted sequencing identified recessive mutations in the *ISPD* gene (encoding isoprenoid synthase domain containing). The pathogenicity of the identified *ISPD* mutations was shown by complementation of fibroblasts with wild-type *ISPD*. Finally, we show that recessive mutations in *ISPD* abolish the initial step in laminin-binding glycan synthesis by disrupting dystroglycan O-mannosylation. This establishes a new mechanism for WWS pathophysiology.

The hallmark of dystroglycanopathies—and the common pathogenic denominator in all individuals with WWS (MIM 236670)—is loss of functional glycosylation of α-dystroglycan[3]. Lack of proper α-dystroglycan glycosylation reduces binding to extracellular matrix proteins, as ligand binding is mediated through the sugar moiety on α-dystroglycan[3,4]. All six of the genes in which causative mutations in WWS have previously been found code for known or putative glycosyltransferases; mutations in these genes show autosomal recessive inheritance patterns and result in abnormal α-dystroglycan glycosylation[5]. Nevertheless, approximately half of the population with WWS has no mutation in these known genes[2], emphasizing the need for discovery of other causative genes that are disrupted in WWS.

We established a complementation assay to enable us to identify additional genes that contribute to WWS pathology. This assay was developed based on a panel of skin fibroblasts derived from six individuals with genetically defined but heterogeneous dystroglycanopathy (**Supplementary Table 1**), in which protein blotting revealed a lack of functional glycosylation (defined as immunoreactivity to IIH6, a monoclonal antibody specific for the requisite sugar moiety) and an inability to bind laminin (**Fig. 1a**). These pathological characteristics are consistent with previously published data obtained from various dystroglycanopathy tissues[3,6] and cells[7–9]. Notably, the degree of α-dystroglycan hypoglycosylation varied with the gene mutated, and the differing molecular weights of α-dystroglycan produced in the individual fibroblast populations are hypothesized to reflect abnormalities at different steps in α-dystroglycan biosynthesis (**Fig. 1a**). In fibroblasts from each population of affected individuals, the α-dystroglycan glycosylation defect was rescued by introducing a wild-type copy of the mutant gene. For example, in fibroblasts from individuals with WWS with known *POMT1* mutations, α-dystroglycan functional glycosylation was restored by adenovirus-mediated gene transfer of *POMT1* but not by expression of the other known WWS-associated genes (**Fig. 1b**). This complementation assay was adapted to On-Cell protein blotting technology, and rescue of α-dystroglycan functional glycosylation was shown for all known WWS-associated genes (**Fig. 1c**).

[1]Department of Molecular Physiology and Biophysics, University of Iowa Roy J and Lucille A Carver College of Medicine, Iowa City, Iowa, USA. [2]Department of Neurology, University of Iowa Roy J and Lucille A Carver College of Medicine, Iowa City, Iowa, USA. [3]Department of Internal Medicine, University of Iowa Roy J and Lucille A Carver College of Medicine, Iowa City, Iowa, USA. [4]Howard Hughes Medical Institute, University of Iowa Roy J and Lucille A Carver College of Medicine, Iowa City, Iowa, USA. [5]Department of Human Genetics, David Geffen School of Medicine, University of California, Los Angeles, California, USA. [6]Department of Pathology and Laboratory Medicine, David Geffen School of Medicine, University of California, Los Angeles, California, USA. [7]Department of Cell Chemistry, Centre for Organismal Studies, University of Heidelberg, Heidelberg, Germany. [8]Dubowitz Neuromuscular Centre, Division of Neuroscience, Institute of Child Health & Great Ormond Street Hospital for Children, London, UK. [9]Molecular Structure and Function, The Hospital for Sick Children, Toronto, Ontario, Canada. [10]Division of Neurology, The Hospital for Sick Children, Toronto, Ontario, Canada. [11]University Pierre et Marie Curie, UM 76, Institut National de la Santé et de la Recherche Médicale (INSERM) U974, Centre Nationale de la Recherche Scientifique (CNRS) Unité Mixte de Recherce (UMR) 7215, Assistance Publoique–Hôpitaux de Paris (AP-HP), Institute of Myology, Paris, France. [12]White-Wilson Medical Center, Fort Walton Beach, Florida, USA. [13]Department of Pediatrics, University of Chicago, Chicago, Illinois, USA. [14]PreventionGenetics, Marshfield, Wisconsin, USA. [15]Department of Pediatrics, University of Iowa Roy J and Lucille A Carver College of Medicine, Iowa City, Iowa, USA. [16]Department of Pathology, University of Iowa Roy J and Lucille A Carver College of Medicine, Iowa City, Iowa, USA. Correspondence should be addressed to K.P.C. (kevin-campbell@uiowa.edu).

Received 8 November 2011; accepted 21 March 2012; published online 22 April 2012; doi:10.1038/ng.2252

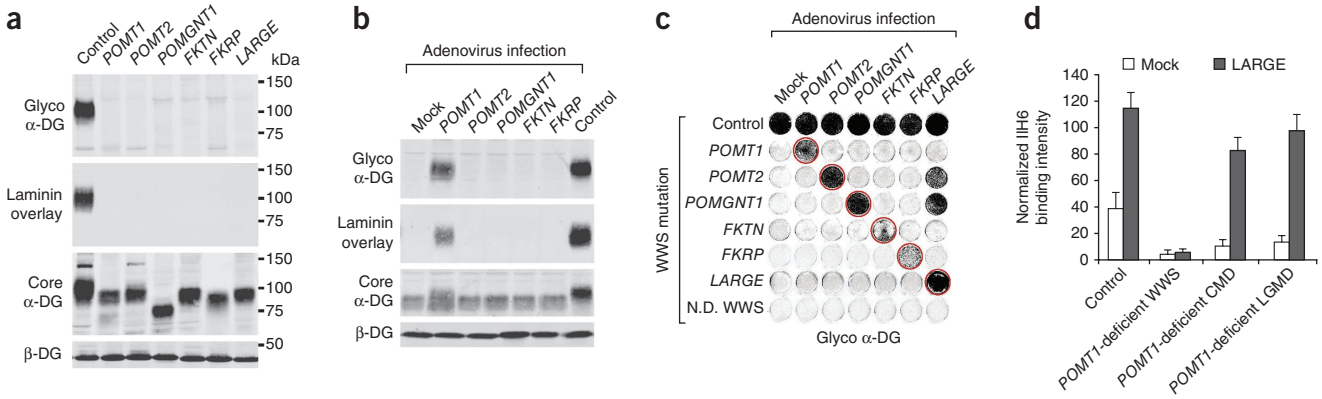

Figure 1 Status of α-dystroglycan glycosylation in dermal fibroblasts from subjects with dystroglycanopathy. Wheat germ agglutinin (WGA)-enriched cell lysates from fibroblasts from control and affected individuals (samples with defects in six different genes; **Supplementary Table 1**) were subjected to biochemical analysis. (**a**) Status of α-dystroglycan glycosylation, as assessed by protein blotting using antibodies to the glycosylated form of α-dystroglycan (glyco α-DG) and core α-dystroglycan (core α-DG) and by laminin overlay assay. An antibody to β-dystroglycan (β-DG) was used to assess loading. (**b**) Complementation assay. Immunoblot of *POMT1*-deficient cells from a subject with WWS infected with a panel of adenoviruses expressing WWS candidate genes; only adenovirus-mediated gene transfer with a wild-type copy of *POMT1* rescues the defect. (**c**) On-Cell protein blot analysis of fibroblasts from control and genetically heterogeneous subjects with WWS shows that the complementation approach, using adenovirus-mediated gene transfer, can successfully be applied to all known WWS-associated genes. Restoration of the glycosylation defect is indicated by a red circle. N.D. WWS, sample from a non-diagnosed person with WWS; lack of rescue suggests a new genetic defect. Note that *LARGE* overexpression rescues and bypasses α-dystroglycan hypoglycosylation in less severe WWS–Muscle Eye Brain (MEB) disease cells with hypothesized residual activity (*POMT2* and *POMGNT1* deficient) but not in cells from subjects with the most severe loss-of-function form of WWS. The On-Cell protein blot was probed with antibody to the glycosylated form of α-dystroglycan, and, for signal enhancement, the cells were coinfected with dystroglycan-expressing adenovirus (Ad5CMV-*DAG1*). (**d**) Quantitative On-Cell protein blot analysis of LARGE-induced α-dystroglycan hyperglycosylation in control and *POMT1*-deficient cells from three subjects with different clinical severity. The ability of LARGE to bypass the glycosylation defect in *POMT1*-deficient cells, resulting in increased affinity of the cell surface for the IIH6 antibody to glycosylated α-dystroglycan, correlates with the residual activity of the mutant gene product and the severity of the clinical manifestation. IIH6 On-Cell quantitative data were normalized with DRAQ5 cell DNA dye ($n = 3$). Error bars, s.d. CMD, congenital muscular dystrophy; LGMD, limb-girdle muscular dystrophy.

Previously, it was shown that forced overexpression of the glycosyltransferase LARGE induces α-dystroglycan hyperglycosylation in control cells and bypasses the α-dystroglycan glycosylation defect in cells from individuals with dystroglycanopathy[8,10]. However, we now show that the ability of LARGE to hyperglycosylate α-dystroglycan is dependent on the availability of O-mannosyl phosphate acceptor sites and correlates with the severity of the clinical phenotype (**Fig. 1d**).

We next applied the On-Cell complementation assay to fibroblasts derived from a cohort of 63 individuals with dystroglycanopathy (**Supplementary Fig. 1**), identifying 11 subjects with WWS in 10 unrelated families who we postulated to have mutations in genes not previously implicated in WWS. Our first step toward defining the genetic basis for WWS in these individuals was to establish complementation groups; to this end, we adapted a cell fusion approach that is commonly used in yeast[11] and that has also proven successful in mammalian cells[12]. Whereas fusion is achieved by mating in the case of yeast cells, polyethylene glycol (PEG)[13] treatment is used to induce fusion in mammalian cells. We hypothesized that fusion between co-cultured cells from affected individuals harboring recessive mutations in the same gene would not rescue the α-dystroglycan glycosylation defect, whereas fusion between cells from affected individuals with independent genetic defects would result in successful rescue. Immunofluorescence analysis identified IIH6-positive fused cells (as indicated by the presence of multiple nuclei) only when two cell lines from genetically different individuals were co-cultured; for example, complementation between *POMT1*- and *FKTN*-deficient fibroblasts from subjects with WWS is shown (**Fig. 2a**). Two-way fusions of WWS-derived cells with mutations in each of the known genes rescued α-dystroglycan glycosylation (data not shown). Application of the

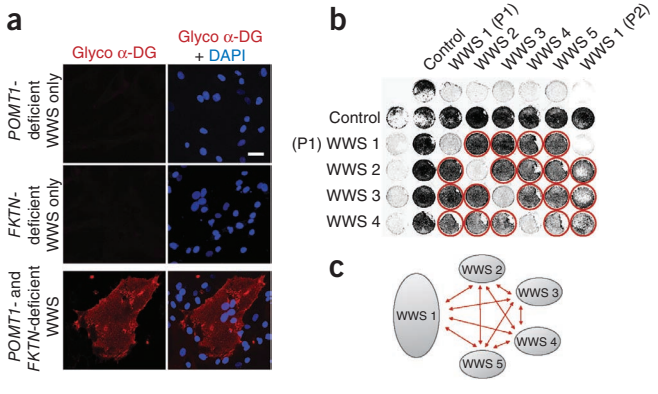

Figure 2 Cell fusion experiments reveal new genetic complementation groups. Cell fusion among co-cultured dermal fibroblasts induced with PEG. (**a**) Immunofluorescence-based detection of restored α-dystroglycan functional glycosylation (glyco α-DG) (scale bar, 50 μm). In contrast to cultures containing only *POMT1*-deficient or *FKTN*-deficient cells from subjects with WWS, co-cultures of these cells exhibited restored functional α-dystroglycan glycosylation in multinucleated cell fusions. Nuclei are stained with DAPI. (**b**) Fibroblasts from a control and five different subjects with WWS with unknown genetic mutations were co-cultured and subjected to cell fusion complementation. Complementation was assessed as rescue of functional α-dystroglycan glycosylation by On-Cell protein blotting. Rescue of the glycosylation defect is indicated by red circles. For signal enhancement, the cells were co-infected with dystroglycan-expressing adenovirus (Ad5CMV-*DAG1*). WWS 1–5, the five new complementation groups. (**c**) Schematic summarizing our identification of five new complementation groups. Red arrows indicate successful fusion complementation. One group (WWS 1) contains seven subjects with WWS, whereas the remaining four groups currently only consist of a single affected person.

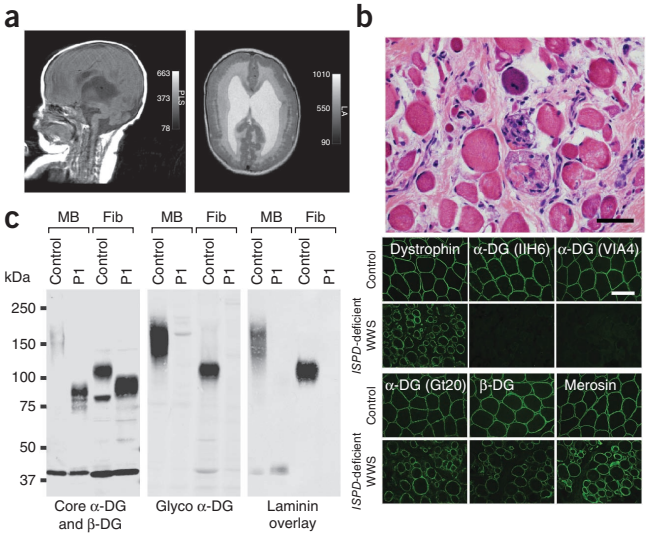

Figure 3 Clinical presentation and α-dystroglycan glycosylation defect in *ISPD*-deficient subject P1 with WWS. (**a**) Sagittal (left) and axial (right) MRI brain images at 5 months of age showed severe ventriculomegaly, agyria and a significantly malformed (Z-shaped) hypoplastic brainstem, as well as severely hypoplastic cerebellar vermis. In addition, the axial image reveals subcortical heterotopia. (**b**) Histological staining of frozen cross-sections from a skeletal muscle biopsy showing severe dystrophic histopathology with muscle fiber necrosis and regeneration, as well as endomysial fibrosis. Top, hematoxylin & eosin. Scale bar, 50 μm. Bottom, immunofluorescence with two antibodies against glycosylated α-dystroglycan (IIH6 and VIA4) reveals a complete loss of functional α-dystroglycan glycosylation. Antibodies against dystrophin, α-dystroglycan core protein (Gt20), β-dystroglycan (β-DG) and laminin α2 (merosin) show mildly reduced to normal staining. Scale bar, 100 μm. (**c**) Protein blot of skeletal muscle biopsy (MB) and skin fibroblasts (Fib) of control and *ISPD*-deficient WWS subject P1. Both samples reveal core α-dystroglycan hypoglycosylation and loss of α-dystroglycan functional glycosylation. Glycoproteins were WGA enriched from muscle or cell lysates (MB, 250 μg protein per lane; Fib, 1,000 μg protein per lane). The immunoblot was probed with antibodies to the glycosylated form of α-dystroglycan (glyco α-DG) and core α-dystroglycan (core α-DG), as well as to β-dystroglycan (β-DG) as a loading control.

PEG fusion approach to all 11 subjects with WWS for whom a genetic cause had not been determined led to the identification of five separate complementation groups (**Fig. 2b**,**c**), suggesting that five new causative genes in WWS were represented in this small cohort. Four complementation groups were represented by a single subject with WWS, and one complementation group consisted of seven subjects with WWS. If mutations in a single newly implicated gene are responsible for disease in all seven subjects, then the genetic alterations in this complementation group likely represent a relatively common cause of WWS.

All seven subjects within this complementation group met the classic diagnostic criteria for WWS (**Supplementary Table 2**). Two of the subjects, P5 (refs. 6,14) and P6 (ref. 15), were described as having WWS in previously published studies. In the case of P1, brain magnetic resonance imaging (MRI) performed at 3 days and at 5 months of age showed hydrocephalus, cobblestone lissencephaly of the cerebral cortex, severe brainstem hypoplasia with a kink at the isthmus and severe hypoplasia of the cerebellum (**Fig. 3a**). This subject also showed evidence of severe muscular dystrophy (**Fig. 3b**), bilateral microphthalmia with cataracts and arrested retinal development. Immunofluorescence and protein blot analysis of a skeletal muscle from this subject showed that individuals in the new WWS complementation group manifested the typical α-dystroglycan glycosylation defect in skeletal muscle, with loss of both functional glycosylation and receptor function (**Fig. 3b**,**c**). Comparative analysis of the status of α-dystroglycan glycosylation in fibroblasts from five different subjects within this same WWS complementation group confirmed that all shared a defect in α-dystroglycan processing, showing complete loss of functional glycosylation and laminin binding (**Supplementary Fig. 2**). Moreover, the loss of post-translational modification of α-dystroglycan and its consequent shift to a lower molecular weight were comparable in all samples, consistent with the hypothesis that individuals from this complementation group share a common genetic defect.

Our first step toward identifying the underlying genetic defect in the large complementation cohort was to perform linkage analysis. As reliable family history regarding consanguinity was not available for all subjects, regions of homozygosity by descent were identified using high-resolution SNP arrays. Besides the sibling pair of subjects P2 and P3, four of the five unrelated subjects showed multiple long (>10 cM) stretches of homozygosity, suggesting some degree of consanguinity (**Supplementary Fig. 3**). We searched for chromosomal regions where P2 and P3 were identical on both alleles and where all or a subset of the four suspected consanguineous subjects were homozygous. All 7,113 coding exons across the 14 identified overlapping intervals were subjected to targeted sequencing (**Supplementary Table 3**). All seven samples were barcoded, pooled, captured by a custom-designed capture array and sequenced on a lane of an Illumina HiSeq2000 flow cell as

Table 1 Summary of pathogenic *ISPD* mutations detected in this study

Subject	Zygosity	Chr.	Genomic position (Build 37)	Nucleotide variant	Amino-acid alteration	
P1	Heterozygous	7	16415758	c.643C>T	p.Gln215*	Nonsense mutation
	Heterozygous	7	g.(16107358–16115680)_(16289931–16297326)del			Deletion of exons 9 and 10
P2 and P3 (siblings)	Heterozygous	7	16348146	c.789+2T>G	Splicing defect	IVS4 splice-site mutation, deletion of exon 4
	Heterozygous	7	16445940	c.277_279del ATT	p.Ile93del	Single amino-acid deletion
P4	Homozygous	7	16131322	c.1354T>A	p.*452Arg	Mutation of original stop codon, next stop codon 27 aa downstream
P5	Homozygous	7	16255823	c.1120–1G>T	Splicing defect	IVS8 splice-site mutation, deletion of exon 9
P6	Homozygous	7	g.(16401191–16406273)_(16409318–16431594)del			In-frame deletion of exon 3
P7	Homozygous	7	16415851	c.550C>T	p.Arg184*	Nonsense mutation

Chr. chromosome.

a total of four heterozygous and four homozygous variants were found in *ISPD* that occurred as multiple rare variants in all six independent affected individuals (**Table 1** and **Supplementary Fig. 4**). All mutations were predicted to damage or abolish protein function, as expected in individuals with a severe form of dystroglycanopathy, such as WWS[7]. In addition, *ISPD* is localized to chromosome 7p21.2, a region in which three of the four suspected consanguineous subjects had intervals of homozygosity longer than 10 cM and where P2 and

a 50-bp paired-end run. Sequence data were processed in a custom-built analysis pipeline, and, after variant filtering was applied, six genes were identified in which at least two independent protein-damaging variants passed hard-filtration criteria (**Supplementary Table 4**). On the basis of genetic evidence, *ISPD* was determined to be the most likely candidate gene. After manually examining variants that did not meet filtration criteria and augmenting the data set with Sanger sequencing results for P5, for whom there was poor coverage,

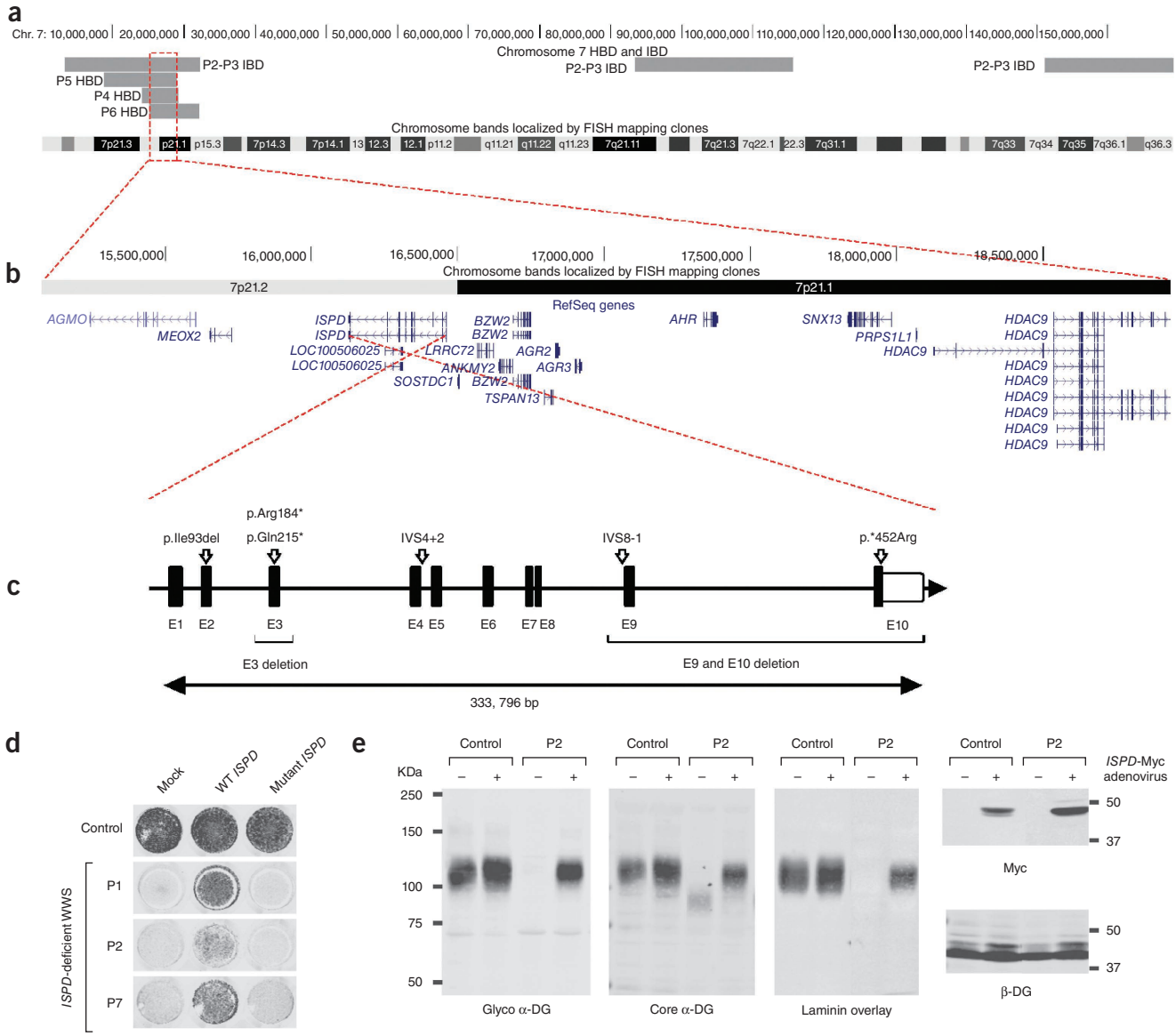

Figure 4 Identification and validation of *ISPD* as a disease-associated gene in subjects with WWS. (**a**) Alignment of identity-by-descent (IBD) and homozygosity-by-descent (HBD) intervals among *ISPD*-deficient subjects on chromosome 7 is shown. Top, genomic position in hg19 coordinates; bottom, chromosome bands. The minimal region of overlap where three of the four samples from suspected consanguineous individuals were homozygous and where P2 and P3 share both parental alleles is highlighted by a red box. (**b**) Genes within the overlap region in **a** are shown in a magnified view. (**c**) Schematic (not to scale) of the *ISPD* exon-intron gene structure. Human *ISPD* cDNA (5,524 bp; NM_001101426) contains 10 coding exons spread across 333,796 bp of genomic DNA. All identified pathogenic ISPD protein changes are indicated, as are regions of exon deletion and splice-site mutations. Coding exons, black boxes; UTRs, open boxes. (**d**) On-Cell protein blot–based complementation assay of fibroblasts from a control and *ISPD*-deficient subject with WWS after nucleofection with a wild-type or mutant *ISPD* expression construct. Rescue of α-dystroglycan functional glycosylation was detected with antibody to glycosylated α-dystroglycan (glyco α-DG). (**e**) Adenovirus-mediated *ISPD* gene transfer rescues the α-dystroglycan glycosylation defect in cells from *ISPD*-deficient subject P2. WGA-enriched cell lysates from fibroblasts were subjected to immunoblotting with antibodies to glycosylated α-dystroglycan (glyco α-DG), core α-dystroglycan (core α-DG), Myc and β-dystroglycan (β-DG) and to laminin overlay. Infection with *ISPD*-Myc adenovirus restored functional glycosylation in *ISPD*-deficient cells from P2 but did not substantially alter α-dystroglycan functional glycosylation in control cells.

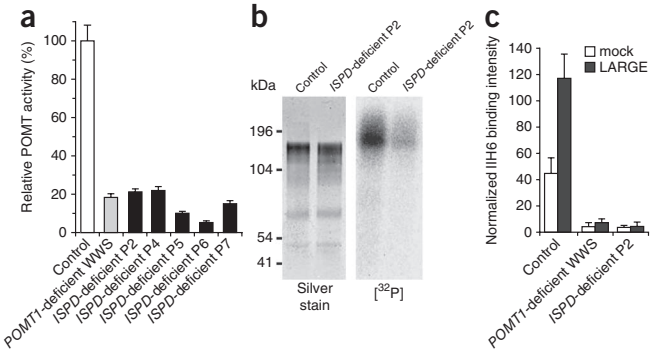

Figure 5 *ISPD* loss-of-function mutations cause α-dystroglycan O-mannosylation defect. (**a**) POMT activity in dermal fibroblasts from a control and affected subjects, as assayed by the rate of [^{3}H]-mannose transfer from dolichol-phosphate-[^{3}H]-mannose (Dol-P-[^{3}H]-Man) (125,000 dpm/pmol) to a GST–α-dystroglycan fusion protein. *POMT1*-deficient and *ISPD*-deficient cells from individuals with WWS show comparable defects in POMT enzyme activity. Specific POMT activity in control cells was determined to be 536.7 pmol/g/h. The diagram shows relative POMT activity in reference to the level detected in control cells ($n = 3$). Error bars, s.d. (**b**) [^{32}P]-orthophosphate labeling of *DGFc5*-expressing cultured cells from a control subject and *ISPD*-deficient cells from P2. After O-mannosyl residues are transferred, [^{32}P]-orthophosphate is incorporated to form a phosphorylated *O*-linked mannose glycan[21]. *ISPD*-deficient cells show markedly reduced orthophosphate labeling due to reduced number of O-mannosyl acceptor sites. (**c**) Quantitative On-Cell protein blot analysis of LARGE-induced α-dystroglycan hyperglycosylation. The glycosyltransferase LARGE participates in a post-phosphoryl modification event transferring the laminin-binding glycan. Forced expression of LARGE increases the affinity of the cell surface for the IIH6 antibody to glycosylated α-dystroglycan in control cells but not in *POMT1*- and *ISPD*-deficient cells from persons with WWS, confirming that the mutant cells lack the O-mannosyl acceptors of the post-phosphoryl modification. On-Cell quantitative data were normalized with DRAQ5 cell DNA dye ($n = 3$). Error bars, s.d.

P3 shared both parental alleles (**Fig. 4a**,**b**). A schematic of all *ISPD* mutations identified in our subject cohort is shown (**Fig. 4c**).

To confirm the pathogenicity of the identified *ISPD* mutations, we conducted complementation assays on fibroblasts derived from the subjects with WWS who had *ISPD* mutations. In the subject-derived cells, expression of wild-type *ISPD* but not that of a mutant isoform (*ISPD* lacking exon 3 from P6) restored functional glycosylation (**Fig. 4d**); in control cells, this overexpression did not substantially alter functional α-dystroglycan glycosylation (**Fig. 4e**). Functional rescue of cells from affected individuals confirmed that the identified *ISPD* mutations have pathogenic relevance and indicated that severe mutations in *ISPD* can cause WWS.

Notably, *ISPD* has not been characterized in mammals. Quantitative RT-PCR (qRT-PCR) revealed that *ISPD* was ubiquitously expressed in all tissues analyzed, with the highest expression occurring in brain (**Supplementary Fig. 5**). The ISPD protein belongs to the family of 4-diphosphocytidyl-2C-methyl-D-erythritol (CDP-ME) synthases (also known as 2-C-methyl-D-erythritol 4-phosphate cytidylyltransferases) that are conserved from bacteria to mammals (**Supplementary Fig. 6**). In *Escherichia coli*, IspD activity contributes to the methylerythritol phosphate (MEP) pathway in the synthesis of isoprenoid precursors[16,17], which give rise to the polyisoprenoid alcohols (for example, dolichols and polyprenols) found in all living organisms[18] (**Supplementary Fig. 7**). However, the MEP pathway is used only by eubacteria, green algae and the chloroplasts of higher plants[19]. Eukaryotes, archaebacteria and the cytosol of higher plants are thought to use an alternative, ISPD-independent mevalonate (MVA) pathway for isoprenoid synthesis[20]. As the MEP pathway involving ISPD is postulated to be absent from animals, the specific role of ISPD in humans, especially in regard to α-dystroglycan glycosylation, is unclear.

To investigate the role of ISPD in α-dystroglycan glycosylation, we tested subjects with WWS who had mutations in *ISPD* for changes in any known step in laminin-binding glycan synthesis. Notably, protein O-mannosylation, the initiating step of this pathway, was markedly reduced in fibroblasts lacking functional ISPD, as were downstream events like O-mannosyl phosphorylation and LARGE-induced hyperglycosylation (**Fig. 5a–c**). These findings suggest that ISPD function is crucial for efficient POMT-dependent O-mannosylation and subsequent glycosylation of α-dystroglycan (**Supplementary Fig. 8**).

In this study, we have identified a new disease-associated gene in individuals with WWS by using a fibroblast complementation assay in combination with targeted sequencing. This approach provided conclusive genetic and biochemical evidence that recessive mutations in *ISPD* lead to impaired α-dystroglycan O-mannosylation, establishing a new pathway and mechanism for disease in WWS. Further studies are needed to determine how mutations in *ISPD* influence protein O-mannosylation, as this is the first WWS-associated gene without proposed glycosyltransferase activity and a direct role in α-dystroglycan glycosylation.

URLs. UCLA Clinical Genomics Center, http://pathology.ucla.edu/body.cfm?id=105; NINDS DNA and Cell Line Repository, http://ccr.coriell.org/ninds; Novocraft Short Read Alignment package, http://www.novocraft.com/index.html; SAMtools, http://samtools.sourceforge.net/; Picard, http://picard.sourceforge.net/; SeattleSeq Annotation, http://snp.gs.washington.edu/SeattleSeqAnnotation131/; ExonPrimer, http://ihg.gsf.de/ihg/ExonPrimer.html.

METHODS

Methods and any associated references are available in the online version of the paper at http://www.nature.com/naturegenetics/.

Note: Supplementary information is available on the Nature Genetics website.

ACKNOWLEDGMENTS

We thank the Gene Transfer Vector Core (University of Iowa, supported by the US National Institutes of Health (NIH) and the National Institute of Diabetes and Digestive and Kidney Diseases (NIDDK) (P30 DK 54759) for generating adenoviruses, T. Toy at the UCLA Clinical Genomics Center (see URLs) for assisting with construction of the sequencing libraries, S. Feng at the UCLA Broad Stem Cell Research Center (BSCRC) for assisting in running HiSeq2000 and B. Harry at the UCLA Clinical Genomics Center for maintaining the data analysis pipeline. Sequencing and sequence analysis were supported by the Center for Duchenne Muscular Dystrophy and the UCLA Muscular Dystrophy Core Center grant from the NIH (5P30AR05723). This study used fibroblast samples from the National Institute of Neurological Disorders and Stroke (NINDS) Cell Line Repository (see URLs) and the Miami Brain and Tissue Bank for Developmental Disorders, funded by the National Commission for Human Development (NICHD). We thank members of the Campbell laboratory and C.A. Campbell for fruitful discussions, A. Dietz, A. Crimmins, G. Morgensen, J. Eskuri, P. Guicheney and H.v. Bokhoven for technical support and C. Blaumueller for critical reading of the manuscript. This work was supported in part by a Paul D. Wellstone Muscular Dystrophy Cooperative Research Center Grant (1U54NS053672 to K.P.C., K.D.M., S.A.M. and T.W.) and an American Recovery and Reinvestment Act (ARRA) Go Grant (1 RC2 NS069521-01 to K.P.C. and T.W.). The Muscular Dystrophy Campaign Grant to F.M. is also gratefully acknowledged. S.C. and F.M. are investigators of and are supported by the European Framework Programme 7 (FP7) NMD-Chip and Bio-NMD projects. F.M. is supported by the Great Ormond Street Hospital Children's Charity. K.P.C. is an investigator of the Howard Hughes Medical Institute.

AUTHOR CONTRIBUTIONS

T.W., H.L., S.F.N. and K.P.C. designed the research. T.W. performed the research and analyzed the data. H.L. and S.F.N. performed SNP analysis, next-generation

sequencing and data filtering. M.L. and S.S. carried out POMT enzyme activity assays. T.Y.-M. performed α-dystroglycan orthophosphate cell labeling experiments. D.B.V.d.B. performed qRT-PCR expression analysis. D.V. carried out antibody affinity purification and labeling. T.L.W. carried out Sanger sequencing of known WWS-associated genes. S.A.M. performed muscle histology and clinical data interpretation. H.S., J.V., S.C., F.M., T.V., A.S.L., W.B.D. and K.D.M. provided clinical data and/or fibroblast samples from individuals with WWS. K.P.C. supervised and mentored the project. T.W. and K.P.C. wrote the initial manuscript, and all authors approved and commented on the manuscript.

COMPETING FINANCIAL INTERESTS

The authors declare no competing financial interests.

Published online at http://www.nature.com/naturegenetics/.
Reprints and permissions information is available online at http://www.nature.com/reprints/index.html.

1. Vajsar, J. & Schachter, H. Walker-Warburg syndrome. *Orphanet J. Rare Dis.* **1**, 29 (2006).
2. Godfrey, C., Foley, A.R., Clement, E. & Muntoni, F. Dystroglycanopathies: coming into focus. *Curr. Opin. Genet. Dev.* **21**, 278–285 (2011).
3. Michele, D.E. *et al.* Post-translational disruption of dystroglycan-ligand interactions in congenital muscular dystrophies. *Nature* **418**, 417–422 (2002).
4. Cao, W. *et al.* Identification of α-dystroglycan as a receptor for lymphocytic choriomeningitis virus and Lassa fever virus. *Science* **282**, 2079–2081 (1998).
5. Barresi, R. & Campbell, K.P. Dystroglycan: from biosynthesis to pathogenesis of human disease. *J. Cell Sci.* **119**, 199–207 (2006).
6. Satz, J.S. *et al.* Brain and eye malformations resembling Walker-Warburg syndrome are recapitulated in mice by dystroglycan deletion in the epiblast. *J. Neurosci.* **28**, 10567–10575 (2008).
7. Lommel, M. *et al.* Correlation of enzyme activity and clinical phenotype in POMT1-associated dystroglycanopathies. *Neurology* **74**, 157–164 (2010).
8. Barresi, R. *et al.* LARGE can functionally bypass α-dystroglycan glycosylation defects in distinct congenital muscular dystrophies. *Nat. Med.* **10**, 696–703 (2004).
9. Clarke, N.F. *et al.* Congenital muscular dystrophy type 1D (MDC1D) due to a large intragenic insertion/deletion, involving intron 10 of the *LARGE* gene. *Eur. J. Hum. Genet.* **19**, 452–457 (2011).
10. Inamori, K. *et al.* Dystroglycan function requires xylosyl- and glucuronyltransferase activities of LARGE. *Science* **335**, 93–96 (2012).
11. Masselot, M. & De Robichon-Szulmajster, H. Methionine biosynthesis in *Saccharomyces cerevisiae*. I. Genetical analysis of auxotrophic mutants. *Mol. Gen. Genet.* **139**, 121–132 (1975).
12. Stanley, P. Membrane mutants of animal cells: rapid identification of those with a primary defect in glycosylation. *Mol. Cell. Biol.* **5**, 923–929 (1985).
13. Pontecorvo, G., Riddle, P.N. & Hales, A. Time and mode of fusion of human fibroblasts treated with polyethylene glycol (PEG). *Nature* **265**, 257–258 (1977).
14. Kanoff, R.J. *et al.* Walker-Warburg syndrome: neurologic features and muscle membrane structure. *Pediatr. Neurol.* **18**, 76–80 (1998).
15. Vajsar, J., Ackerley, C., Chitayat, D. & Becker, L.E. Basal lamina abnormality in the skeletal muscle of Walker-Warburg syndrome. *Pediatr. Neurol.* **22**, 139–143 (2000).
16. Skorupinska-Tudek, K. *et al.* Contribution of the mevalonate and methylerythritol phosphate pathways to the biosynthesis of dolichols in plants. *J. Biol. Chem.* **283**, 21024–21035 (2008).
17. Richard, S.B. *et al.* Structure of 4-diphosphocytidyl-2-C-methylerythritol synthetase involved in mevalonate-independent isoprenoid biosynthesis. *Nat. Struct. Biol.* **8**, 641–648 (2001).
18. Surmacz, L. & Swiezewska, E. Polyisoprenoids—secondary metabolites or physiologically important superlipids? *Biochem. Biophys. Res. Commun.* **407**, 627–632 (2011).
19. Kuzuyama, T. Mevalonate and nonmevalonate pathways for the biosynthesis of isoprene units. *Biosci. Biotechnol. Biochem.* **66**, 1619–1627 (2002).
20. Miziorko, H.M. Enzymes of the mevalonate pathway of isoprenoid biosynthesis. *Arch. Biochem. Biophys.* **505**, 131–143 (2011).
21. Yoshida-Moriguchi, T. *et al.* O-Mannosyl phosphorylation of α-dystroglycan is required for laminin binding. *Science* **327**, 88–92 (2010).

ONLINE METHODS

Subjects and samples. We obtained and tested all tissues and cells from affected persons in agreement with the guidelines set out by the Human Subjects Institutional Review Board of the University of Iowa; informed consent was obtained from all subjects or their legal guardians. More detailed information on fibroblasts from controls and affected individuals with dystroglycanopathy with known genetic defects is summarized in **Supplementary Table 1**.

Cell culture. Cells were maintained at 37 °C and 5% CO_2 in DMEM medium supplemented with 20% FBS and 0.5% penicillin-streptomycin (Invitrogen).

Biochemical analyses. The monoclonal antibodies to the fully glycosylated form of α-dystroglycan (IIH6 and VIA4)[22] and to β-dystroglycan (AP83)[23] have been characterized previously. Gt20 antibody (to core α-dystroglycan) from goat antiserum was raised against the dystrophin-glycoprotein complex (DGC) in its entirety and purified against a hypoglycosylated full-length α-dystroglycan–human IgG Fc fusion protein[3,24]. Additionally, antibodies against the protein backbone of α-dystroglycan were generated by injecting a keyhole limpet hemocyanin (KLH)-conjugated synthetic peptide consisting of amino acids 485–514 of human dystroglycan (Swiss-Prot Q14118) into rabbits (G6317, Genemed Biosynthesis). The antibody to core α-dystroglycan was affinity purified using BSA-conjugated C-terminal peptide[25]. Mouse monoclonal antibody to Myc (4A6) was purchased from Millipore.

Assay for protein O-mannosyltransferase activity. Protein O-mannosyltransferase activity was determined on the basis of the amount of [^{3}H]-mannose transferred from Dol-P-[^{3}H]-mannose to an α-dystroglycan glutathione-S-transferase fusion, as described elsewhere[7,26].

[^{32}P]-orthophosphate labeling of cells. Phosphorylation of α-dystroglycan in fibroblasts from affected individuals was determined on the basis of the incorporation of [^{32}P] into a secreted Fc-tagged α-dystroglycan recombinant protein (DGEc5), as described elsewhere[21].

Adenovirus generation and gene transfer. E1-deficient recombinant adenoviruses (Ad5CMV-*DAG1*, Ad5CMV-DGFc5, Ad5CMV-*POMT1*/RSVeGFP, Ad5CMV-*POMT2*/RSVeGFP, Ad5CMV-*POMGnT1*/RSVeGFP, Ad5CMV-*FKTN*/RSVeGFP, Ad5CMV-*FKRP*/RSVeGFP and Ad5CMV-*LARGE*/RSVeGFP) were generated by the University of Iowa Gene Transfer Vector Core and described previously[8,27]. Similarly, Ad5CMV-*ISPD*-Myc/RSVeGFP was generated by cloning the ORF corresponding to human *ISPD* (NM_001101426) in frame with a sequence encoding a C-terminal Myc tag into the polylinker region of pAd5CMVK-NpA. Cell cultures were infected with viral vector for 12 h at an MOI of 400. We examined cultures 3–5 d after treatment. We also used nucleofection as a non-viral method for gene transfer into cells. Nucleofection of fibroblasts was performed using the Human Dermal Fibroblast Nucleofector Kit, according to an optimized protocol provided by the manufacturer (Amaxa Biosystems).

***ISPD* expression vector construction.** cDNA was generated from fibroblasts from a control individual and from subject P6 with *ISPD*-deficient WWS (in-frame deletion of exon 3, 50 aa deletion) fibroblasts. The C-terminally Myc-tagged coding regions of human wild-type *ISPD* (1,395 bp) and mutant *ISPD* (1,245 bp) were amplified from cDNA by PCR, using primer pair 7717/7718 (**Supplementary Table 5**). The amplified PCR product was subcloned using the pcDNA3.1/V5-His TOPO TA Expression Kit (Invitrogen).

Immunohistochemical analysis. Cryosections of skeletal muscle biopsies (10 μm thick) were processed for immunofluorescence as described[23]. Mouse monoclonal antibody to laminin α2 (anti-merosin, clone 5H2) was purchased from Millipore. Cultured cells were fixed in 4% paraformaldehyde for 10 min and permeabilized with 0.1% Triton X-100 in PBS for 10 min, before being blocked and incubated with primary antibody. Slides were visualized on an Axio Imager.M1 microscope (Zeiss).

Glycoprotein enrichment and biochemical analysis. WGA-enriched glycoproteins of frozen samples and cultured cells were processed as described[3]. Immunoblots were performed on PVDF membranes as described[3]. Blots were developed with infrared (IR) dye–conjugated secondary antibodies (Pierce) and scanned with an Odyssey infrared imaging system (LI-COR Bioscience). Laminin overlay assays were performed as previously described[3].

On-Cell complementation assay of fibroblasts from subjects with WWS. Cells (2×10^5) were seeded into a 48-well dish. The next day, cells were co-infected with Ad5CMV-*DAG1* at an MOI of 200 for signal enhancement and Ad5 complementation constructs at an MOI of 200 (except for Ad5CMV-*FKRP*/RSVeGFP, which was used at an MOI of 40) in growth medium. After 4 d, the cells were washed in TBS and fixed with 4% paraformaldehyde in TBS for 10 min. After blocking with 3% dry milk in TBS with 0.1% Tween (TBS-T), the cells were incubated with primary antibody (to glycosylated α-dystroglycan, IIH6) in blocking buffer overnight. For developing the On-Cell protein blots, we conjugated goat antibody to mouse IgM (Millipore) with IR800CW dye (LI-COR), subjected the sample to gel filtration and isolated the labeled antibody fraction. After staining with IR800CW-labeled secondary antibody in blocking buffer, cells were washed in TBS, and we scanned the 48-well plate with an Odyssey infrared imaging system. For cell normalization, DRAQ5 cell DNA dye (Biostatus Limited) was added during incubation with the secondary antibody.

PEG-induced fusion of dermal fibroblasts. Cell fusion assays were performed as published previously[28]. In brief, cells were seeded into a 48-well dish or onto a tissue culture chamber slide. When the cells reached 90–100% confluency, the culture medium was removed, and cell fusion was induced by adding 55% PEG1500 in DMEM to the cell monolayer and incubating for 1 min at room temperature. The fusion solution was then discarded, and the cell monolayer was rapidly rinsed four times with complete growth medium at room temperature and then returned to the 37 °C tissue culture incubator. The next day, fusion-induced cells were infected with Ad5CMV-*DAG1* at an MOI of 200 for signal enhancement. After 4 d, cells were fixed and stained.

Linkage analysis. Genomic DNA samples were genotyped on an Illumina Omni-1 Quad BeadChip. Identity-by-descent (IBD) and homozygosity-by-descent (HBD) analyses were performed using a custom Mathematica script (Wolfram Research: B. Merriman, available on request), which compared genomes for genotype identity and identified long intervals of homozygosity[29].

Targeted next-generation sequencing. Regions over 10 cM in length where the sibling pair of P2 and P3 showed IBD for both alleles were selected, as were regions that were homozygous for over 2 cM in one or more of the four samples suspected to come from consanguineous individuals (P4, P5, P6 and P7), and were used to create a custom capture array. Using Agilent eArray, a 244K comparative genomic hybridization (CGH) array was designed to target in total 7,113 coding exons across 14 overlapping intervals (**Supplementary Table 3**). Repeat regions were excluded. Genomic DNA (3 μg) was used to generate each sequencing library, using the Agilent SureSelect Target Enrichment System for Illumina Paired-End Sequencing Library Protocol (version 2.0.1); the only difference was that seven different custom-made, barcoded adaptors were used in place of the commercially available adaptor (sequences available on request). After amplification, samples were pooled at equal molar concentrations, captured on one array following an in-house protocol[30] and sequenced on the Illumina HiSeq2000 as 50-bp paired-end reads.

Sequence read alignment. Barcodes were removed from sequence reads, and sequences were aligned to the Human reference genome Build 37 (hg19) using Novobarcode and Novoalign from the Novocraft Short Read Alignment Package (see URLs). Data were processed with SAMtools (version 0.1.15, see URLs)[31], and potential PCR duplicates were removed using Picard (see URLs). The mean coverage achieved within the intended captured region was 35.9× per base, with 82.2% of the targeted base pairs covered at ≥10×. Local realignment was performed using the GATK[32,33] IndelRealigner tool.

Variant calling. Variants were called using the GATK Unified Genotyper tool simultaneously for all seven samples. Small indels were called with the -glm

DINDEL option. Variants with a phred-scaled *Q* score of ≥50.0 were reported as PASSed calls, and those with a *Q* score of ≥10.0 and <50.0 were reported as Low Qual calls. Using the GATK VariantFiltrationWalker tool, both SNPs and indels were hard filtered to eliminate low-quality variants. The following filtering parameters were used, which were suggested to be standard by GATK, to remove likely false positive variants: (i) clusterWindowSize of 10, (ii) mapping quality of zero (MAPQ0) of >40, (iii) quality-by-depth (QD) of <5.0 and (iv) strand bias (SB) >−0.10. The GATK VariantEval tool was used to collect the statistics for the PASSed variants (**Supplementary Table 6a**).

Variant annotation. PASSed variants that were not found in dbSNP132 were annotated using SeattleSeq Annotation version 6.16 (see URLs); single-nucleotide variants (SNVs) and indels were annotated separately. Variants present in the 1000 Genomes Project database (March 2010 release) or dbSNP131, as well as those that resulted in coding synonymous changes or affected sequences outside of a coding region, were removed from further analysis (**Supplementary Table 6b**). The remaining 84 variants were prioritized on the basis of the frequency of coexistence within the same gene.

Copy-number variant (CNV) detection. To identify exonic deletions within the *ISPD* gene, the log R ratio (LRR) of the coverage (Cov), $Cov_{i,j}$ / $Cov_{i,P4}$ was calculated for each exon *i* in each sample *j* using ExomeCNV with subject P4 as a control[31].

Sanger sequencing. Genomic DNA was extracted from dermal fibroblasts or transformed lymphoblastoid cell lines using standard methods (Qiagen DNeasy Blood & Tissue Kit). Coding regions (ten exons) and exon-intron boundaries of *ISPD* were amplified using PCR (primers sequences and PCR conditions are available upon request). Primer sets for PCR were designed using the web-based design tool ExonPrimer. After PCR amplification, purified products were evaluated by Sanger sequencing using standard protocols.

22. Ervasti, J.M. & Campbell, K.P. Membrane organization of the dystrophin-glycoprotein complex. *Cell* **66**, 1121–1131 (1991).
23. Duclos, F. *et al.* Progressive muscular dystrophy in α-sarcoglycan–deficient mice. *J. Cell Biol.* **142**, 1461–1471 (1998).
24. Kunz, S., Sevilla, N., McGavern, D.B., Campbell, K.P. & Oldstone, M.B. Molecular analysis of the interaction of LCMV with its cellular receptor α-dystroglycan. *J. Cell Biol.* **155**, 301–310 (2001).
25. Sharp, A.H. & Campbell, K.P. Characterization of the 1,4-dihydropyridine receptor using subunit-specific polyclonal antibodies. Evidence for a 32,000-Da subunit. *J. Biol. Chem.* **264**, 2816–2825 (1989).
26. Manya, H. *et al.* Demonstration of mammalian protein O-mannosyltransferase activity: coexpression of POMT1 and POMT2 required for enzymatic activity. *Proc. Natl. Acad. Sci. USA* **101**, 500–505 (2004).
27. de Bernabé, D.B. *et al.* Loss of α-dystroglycan laminin binding in epithelium-derived cancers is caused by silencing of *LARGE*. *J. Biol. Chem.* **284**, 11279–11284 (2009).
28. Davidson, R.L. & Gerald, P.S. Improved techniques for the induction of mammalian cell hybridization by polyethylene glycol. *Somatic Cell Genet.* **2**, 165–176 (1976).
29. Lee, H., Jen, J.C., Cha, Y.H., Nelson, S.F. & Baloh, R.W. Phenotypic and genetic analysis of a large family with migraine-associated vertigo. *Headache* **48**, 1460–1467 (2008).
30. Lee, H. *et al.* Improving the efficiency of genomic loci capture using oligonucleotide arrays for high throughput resequencing. *BMC Genomics* **10**, 646 (2009).
31. Li, H. *et al.* The Sequence Alignment/Map format and SAMtools. *Bioinformatics* **25**, 2078–2079 (2009).
32. McKenna, A. *et al.* The Genome Analysis Toolkit: a MapReduce framework for analyzing next-generation DNA sequencing data. *Genome Res.* **20**, 1297–1303 (2010).
33. DePristo, M.A. *et al.* A framework for variation discovery and genotyping using next-generation DNA sequencing data. *Nat. Genet.* **43**, 491–498 (2011).

Supplementary Information

ISPD loss-of-function mutations disrupt dystroglycan *O*-mannosylation and cause Walker-Warburg syndrome

Tobias Willer, Hane Lee, Mark Lommel, Takako Yoshida-Moriguchi, Daniel Beltran Valero de Bernabe, David Venzke, Sebahattin Cirak, Harry Schachter, Jiri Vajsar, Thomas Voit, Francesco Muntoni, Andrea S. Loder, William B. Dobyns, Thomas L. Winder, Sabine Strahl, Katherine D. Mathews, Stanley F. Nelson, Steven A. Moore, Kevin P. Campbell*

* correspondence should be addressed to K.P.C.: kevin-campbell@uiowa.edu

Nature Genetics: doi:10.1038/ng.2252

Supplementary Figure 1

a

Genetic defect	WWS	MEB/FCMD	CMD	total	total %
POMT1	8		5	13	21%
POMT2	1	6	5	12	19%
POMGnT1	1	9	3	13	21%
FKTN	1	4	3	8	13%
FKRP	1		4	5	8%
LARGE			1	1	1%
n.d.	11 (incl.7 *ISPD*)			11	17%
total	23	19	21	63	100%
total %	37%	30%	33%	100%	

b

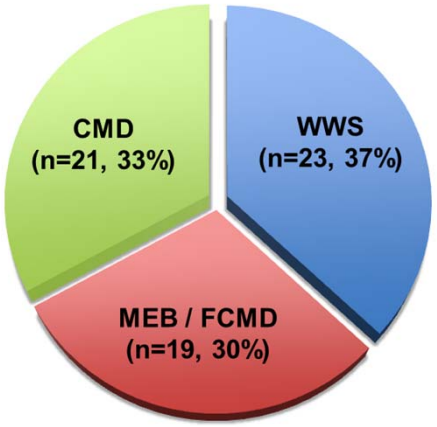

c

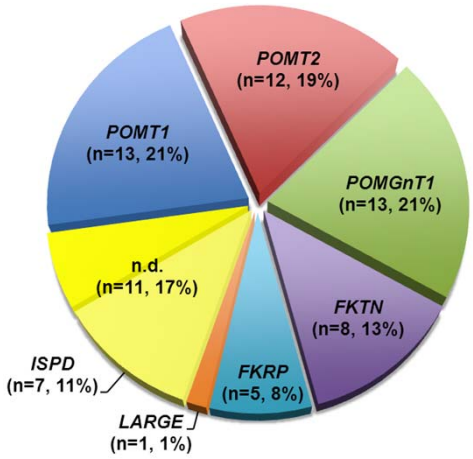

Supplementary Figure 1. Genetic and phenotypic distribution of dystroglycanopathy patient fibroblasts analyzed by On-Cell western blot complementation
(**a**) The table summarizes the On-Cell complementation assay results from 63 patient fibroblasts. Listed are the phenotypic distribution and mutation frequencies in each of the six glycosyltransferase genes within our patient cohort. (**b**) Pie chart representing the phenotypic distribution of patients analyzed by On-Cell complementation assay. (**c**) Pie chart representing the mutation frequencies in the patients analyzed by On-Cell complementation assay. The mutation frequencies of each candidate gene roughly correlate with previously published data by Godfrey *et al.* (2007)[1].

Supplementary Figure 2

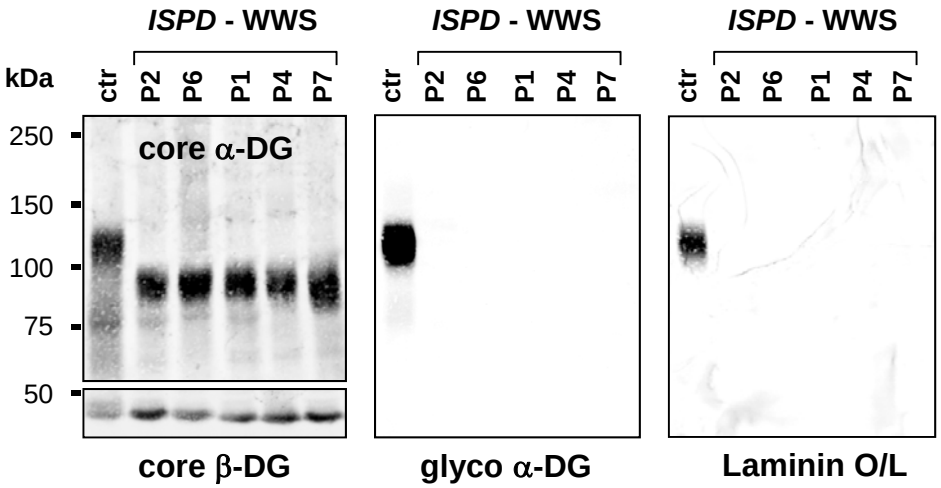

Supplementary Figure 2. Western blot with WGA enriched glycoproteins from five WWS patients in complementation group 1
Comparison of fibroblast α-DG glycosylation status reveals complete loss of functional α-DG glycosylation and a comparable hypoglycosylation of core α-DG in all patient samples. Immunoblot was probed with antibodies against the glycosylated form of α-DG (IIH6), core α-DG (G6317), and β-DG (AP83) as loading control. Receptor binding activity was analyzed with Laminin binding overlay assay.

Nature Genetics: doi:10.1038/ng.2252

Supplementary Figure 3

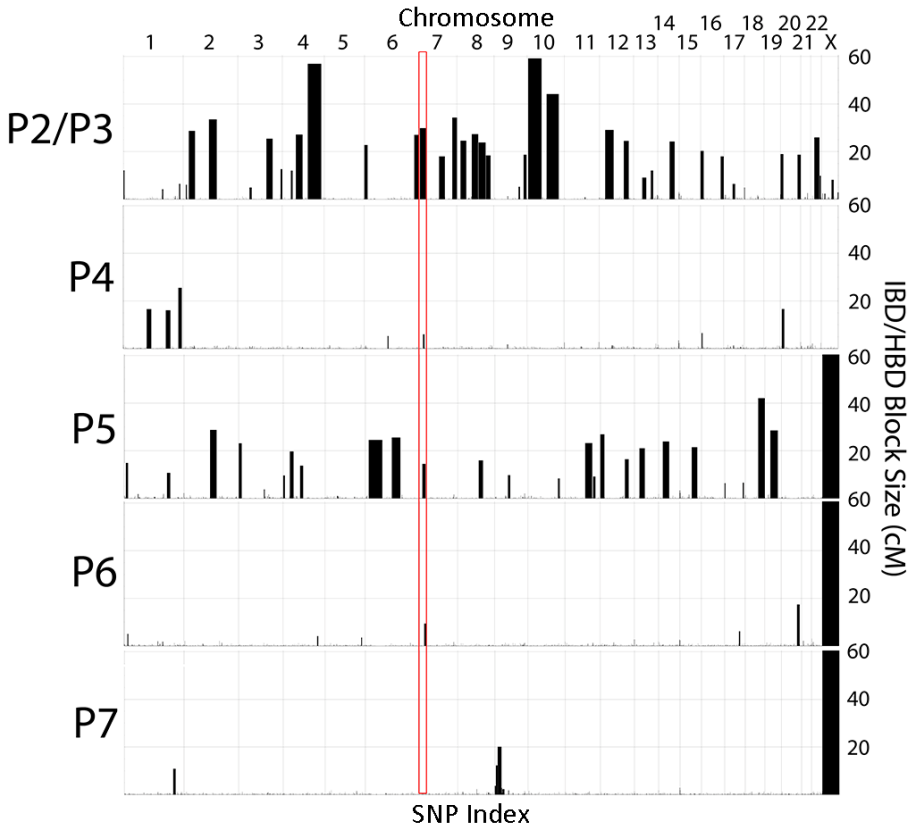

Supplementary Figure 3. Alignment of identical-by-descent (IBD) and homozygosity-by-descent (HBD) intervals among *ISPD* deficient patients. IBD or HBD block size is plotted according to cM along the y-axis, and according to SNP index along the x-axis. The ratio of the width of the block to the height of the block indicates the SNP density (# of SNPs/cM) within the interval. A region on chromosome 7 where three out of four suspected consanguineous samples are homozygous while overlapping with the P2/P3 Z2 region is highlighted by a red box.

Nature Genetics: doi:10.1038/ng.2252

Supplementary Figure 4

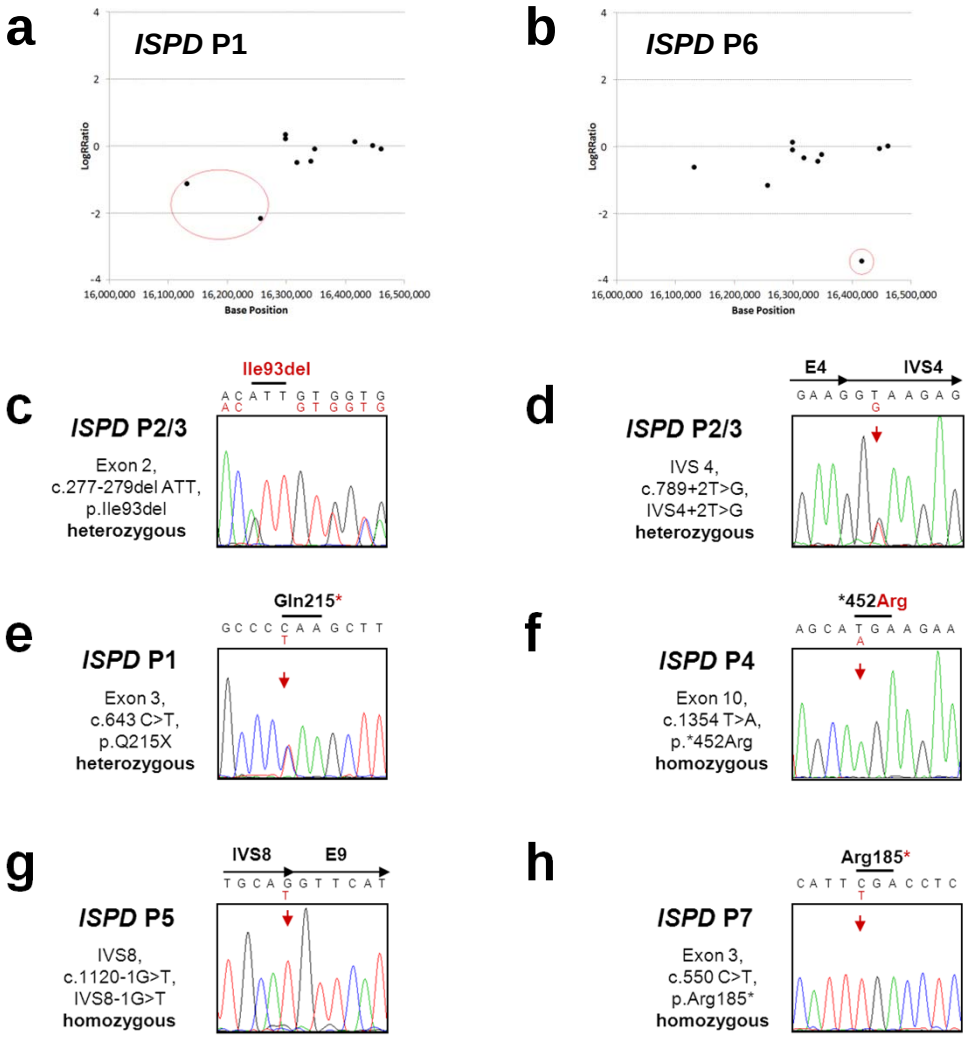

Supplementary Figure 4. Genomic sequence analysis of *ISPD* deficient patients LogRratio (LRR) reveals large exonic deletions in *ISPD* P1 and *ISPD* P6. The deletions were supported by the Illumina Omni-1 genotyping data. (**a**) *ISPD* P1: 53 contiguous SNPs spanning the two exons were all homozygous. The most outward boundaries of this heterozygous deletion were determined by the flanking SNPs of the 53 homozygous SNPs (rs1528149 and rs9918580), predicting the deletion could be up to 190 kb in size. (**b**) *ISPD* P6: Three SNPs near exon 3 (rs12699786, rs12671637, rs10237809) were not called while these SNPs were called with high confidence in the other 7 samples. The most outward boundaries of this homozygous deletion were determined by the flanking SNPs of the 3 SNPs not called (rs7789712 and rs11972185). (**c-g**) Sanger sequencing of *ISPD* deficient patients. Chromatograms with genomic DNA sequence variations are shown for *ISPD* patients P2/3 (**c,d**), P1 (**e**), P4 (**f**), P5 (**g**) and P7 (**h**).

Nature Genetics: doi:10.1038/ng.2252

Supplementary Figure 5

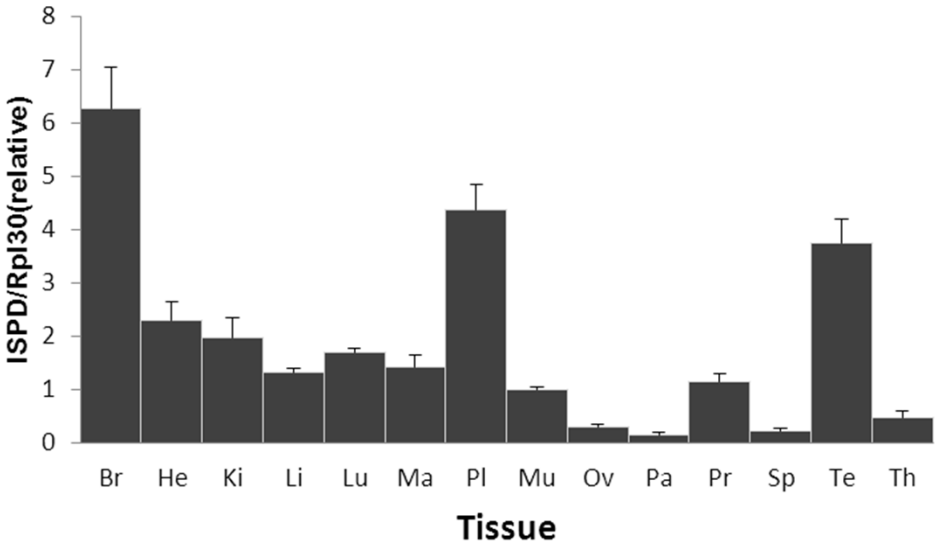

Supplementary Figure 5. qPCR expression analysis of *ISPD* in human tissues
ISPD shows ubiquitous expression in all tissues analyzed. Highest *ISPD* expression was detected in brain. For normalization ribosomal protein Rpl30 was used. Analyzed tissues: Br (brain), He (heart), Ki (kidney), Li (liver), Lu (lung), Ma (mammary gland), Pl (placenta), Mu (skeletal muscle), Ov (ovary), Pa (pancreas), Pr (prostate), Sp (spleen), Te (testis), Th (thymus)

Nature Genetics: doi:10.1038/ng.2252

Supplementary Figure 6

a

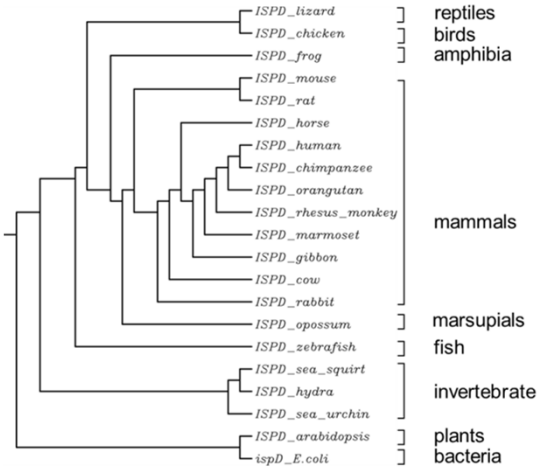

b

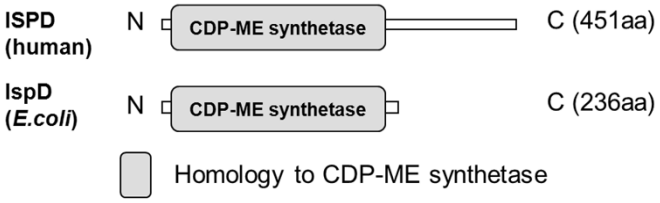

c

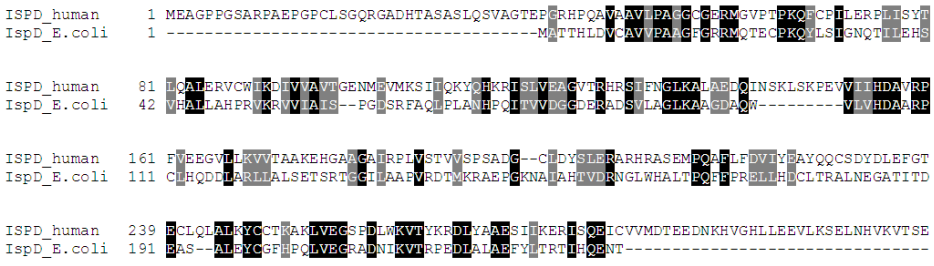

Supplementary Figure 6. ISPD conservation across species
(**a**) Phylogenic tree of ISPD proteins from different species. ISPD proteins are conserved from men to bacteria. Interestingly, no ISPD homologs are present in flies *(Drosophila melanogaster)* and nematodes *(Caenorhabditis elegans).* The dendrogram was generated using ClustalW sequence alignment. (**b**) Schematic representation of human and *E.coli* ISPD proteins. The shared proposed CDP-ME synthase catalytic domain is highlighted with a grey box. (**c**) Protein sequence alignment of protein ISPD sequences from human and *E.coli*. Both proteins sequence share 26% identity and 44% similarity. Identical amino acids are highlighted in black and similar amino acids are highlighted in grey.

Nature Genetics: doi:10.1038/ng.2252

Supplementary Figure 7

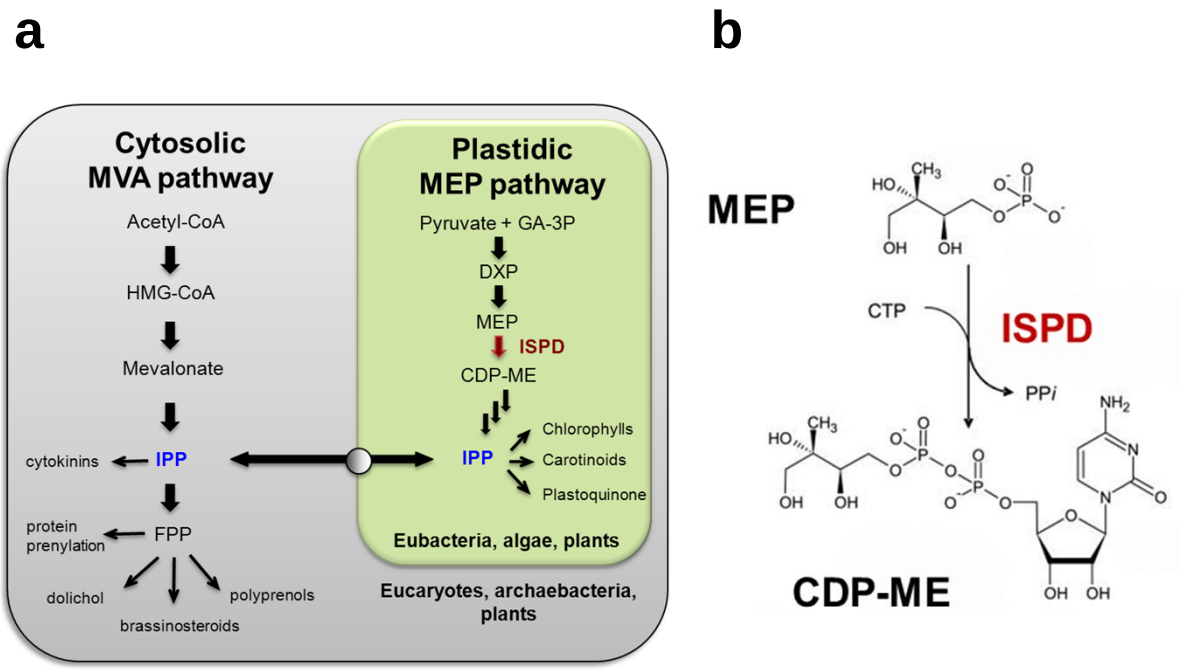

Supplementary Figure 7. ISPD is involved in the MEP pathway for isoprenoid precursor synthesis

(**a**) Schematic representation of the isoprenoid precursor synthesis which differs in human, plant and bacteria (adapted from Rodríguez-Concepción and Boronat, 2002)[2] . Mammals only use the MVA pathway, bacteria only use the MEP pathway, while plants use both pathways spatially separated in the cytoplasm and plastids. In plants both pathways are interconnected through the intermediate IPP (isopentenyl diphosphate, highlighted in blue). The biosynthetic step catalyzed by ISPD is highlighted in red. (**b**) 4-diphosphocytidyl-2-C-methyl-D-erythritol synthase (ISPD) catalyzes the formation of 4-diphosphocytidyl-2-C-methyl-D-erythritol (CDP-ME) from 2-C-methyl-D-erythritol 4-phosphate (MEP) and CTP.

Nature Genetics: doi:10.1038/ng.2252

Supplementary Figure 8

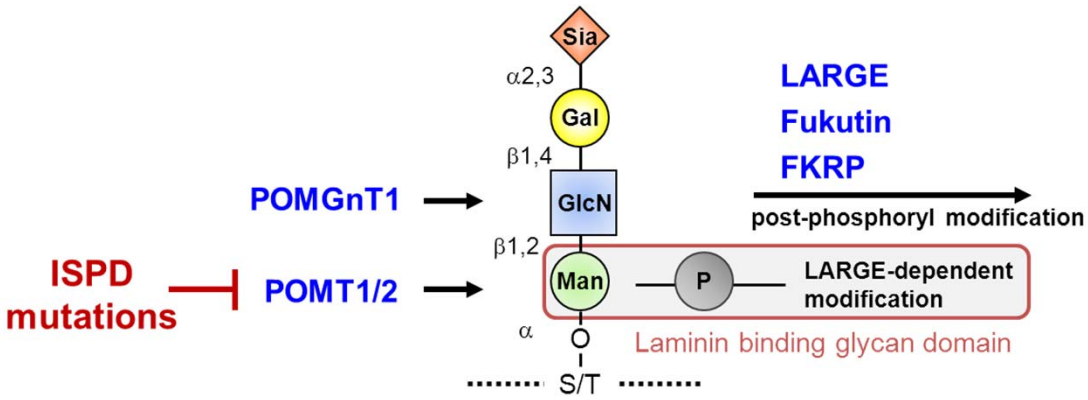

Supplementary Figure 8. ISPD mutations impair protein *O*-mannosylation resulting in loss of laminin binding glycan
Schematic representation of the α-DG functional glycan and the known WWS gene products (indicated in blue) that are involved in its synthesis. ISPD defects impair protein *O*-mannosylation, which is the initial step in the synthesis of the laminin binding glycan. LARGE, Fukutin and FKRP are postulated to be involved in the post-phoshoryl modification.

Nature Genetics: doi:10.1038/ng.2252

Supplementary Table 1

Mutant gene	Clinical phenotype	Zygosity	Nucleotide variant	Amino acid	Reference
Control	n.d.				CRL-2127 (ATCC)
POMT1	WWS	heterozygous	c.997C>T c.1006T>G	p.Pro273Leu p.Leu276Arg	
POMT1	CMD	heterozygous	c.85A>C c.1864C>T	p.Ser29Arg p.Arg622*	
POMT1	LGMD	heterozygous	c.512T>G genomic deletion of exon 18-19	p.Leu171Arg p.Ala589Val fs*38	[3]
POMT2	WWS/MEB	heterozygous	c.1116+1G>A c.1997A>G	p.Gln372fs p.Tyr666Cyc.	
POMGnT1	WWS/MEB	heterozygous	c.794G>A c.932G>A	p.Arg265His p.Arg311Gln	
FKTN	WWS	heterozygous	c.385delA c.1176C>A	p.Ile129fs*1 p.Tyr392*	GM16192 (Coriell Cell Repository)
FKRP	WWS	homozygous	c.1A>G	p.Met1Val	[4]
LARGE	CMD	homozygous	large intra-chromosomal duplication inserted into intron 10		[5]

Supplementary Table 1. Summary of control and dystroglycanopathy patient fibroblast cell lines

Nature Genetics: doi:10.1038/ng.2252

Patient	Phenotype	Life span	α-DG functional glycosylation	Muscle	Brain	Eye	Reference
P1	WWS	15 months	IIH6 negative	biopsy at 12 months dystrophic, CK 3,000 to 13,000 U/l	MRI at 3 days and 5 months: hydrocephalus, cobblestone lissencephaly, beaded subcortical heterotopia, thin corpus callosum, increased white matter signal, brainstem hypoplasia, cerebellar hypoplasia	bilateral microphthalmia and cataracts, arrested retinal development	
P2	WWS	16 months	IIH6 negative	no biopsy, CK 5,400 U/l	MRI at 1 day: hydrocephalus with marked thinning of cortex, cobblestone lissencephaly, brain stem atrophy	bilateral microphthalmia with cataract, persistent hyperplastic primary vitreous, retinal detachment	
P3	WWS	24 months	IIH6 negative	no biopsy, CK 3,300 U/l	MRI at 1 day: massive hydrocephalus, cerebellar hypoplasia, cobblestone lissencephaly	bilateral optic nerve hypoplasia, loss of macular pigment	
P4	WWS	unknown	IIH6 negative	unknown	unknown	unknown	Case #1980, Miami Brain and Tissue Bank for Developmental Disorders
P5	WWS	6 months	IIH6 negative	biopsy at 1 month dystrophic, CK 2,927 U/l	MRI and autopsy: hydrocephalus, agyria, cobblestone lissencephaly, beaded subcortical heterotopia, thin corpus callosum, brainstem hypoplasia, cerebellar hypoplasia	unilateral microphthalmia with cataract, optic nerve hypoplasia	Case #1001, Miami Brain and Tissue Bank for Developmental Disorders[6,7]
P6	WWS	3 months	IIH6 negative	dystrophic, CK 9,577 U/l	MRI and autopsy: hydrocephalus, agyria/pachygyria, cobblestone lissencephaly, cerebellar hypoplasia	Peters' anomaly, retinal detachment, cornea dysplasia	[8,9]
P7	WWS	unknown	IIH6 negative	dystrophic, CK 6,126 U/l	MRI: cobblestone lissencephaly with partial pachygyria, hydrocephalus, partial agenesis of corpus callosum, brainstem hypoplasia, cerebellar hypoplasia	unilateral congenital cataract, focal corneal clouding	

Supplementary Table 2. Clinical characteristics of *ISPD* deficient WWS cases

Nature Genetics: doi:10.1038/ng.2252

Supplementary Table 3

Chromosome	Intervals targeted for sequencing (b37)	No. of families HBD/IBD at the interval	No. exons targeted
chr2	110,443,753-142,636,523	2	1,766
chr4	114,226,988-131,107,545	2	600
chr4	157,486,220-163,245,174	2	176
chr4	25,531,234-35,429,711	2	202
chr4	71,520,178-86,932,486	2	1,027
chr7	15,066,544-18,938,376	4	157
chr8	70,942,229-72,095,586	2	66
chr8	84,739,785-103,732,048	2	1,029
chr9	130,884,753-131,640,165	2	249
chr10	112,562,802-119,178,574	2	556
chr12	100,576,725-104,925,884	2	415
chr16	3,301,360-6,149,092	2	498
chr20	4,195,591-7,256,082	2	154
chr20	53,875,809-57,914,046	2	218

Supplementary Table 3. List of all targeted intervals for sequencing and the number of families that were HBD or IBD and the number of exons targeted at each interval are shown.

Nature Genetics: doi:10.1038/ng.2252

Supplementary Table 4

Number of Variants	Gene symbol	Gene name	Process involved according to Gene Ontology Annotation Database
4	***ISPD***	isoprenoid synthase domain containing	isoprenoid biosynthetic process
3	***PABPC1***	Polyadenylate-binding protein 1	RNA metabolic process
3	***LRP1B***	Low-density lipoprotein receptor-related protein 1B	protein transport, receptor-mediated endocytosis
2	***SCTR***	secretin receptor	G-protein coupled receptor signaling pathway
2	***THSD7B***	thrombospondin, type I, domain containing 7B	biological process unknown
2	***POP1***	processing of precursor 1, ribonuclease P/MRP subunit	RNA processing

Supplementary Table 4. Genes with multiple functional variants that PASSed the hard-filtration in the targeted sequencing data

Nature Genetics: doi:10.1038/ng.2252

Supplementary Table 5

primer	sequence	comment
7717	5'-ATGgaggccgggccgccgg-3'	forward primer, start ATG is capitalized
7718	5'-**cta**CAAGTCTTCTTCAGAAATAAGTTTTTGTTC gctagcccctgctatcagaagctgaccaatg-3'	reverse primer, myc-tag is capitalized, STOP codon is highlighted in bold

Supplementary Table 5. Primers for human *ISPD* cloning

Nature Genetics: doi:10.1038/ng.2252

Supplementary Table 6

a

			P1	P2	P3	P4	P5	P6	P7
SNV	No of variants	All	684	688	689	667	567	670	674
		Known*	669	667	668	637	555	647	656
		Novel†	15	21	21	30	12	23	18
		dbSNP132_rate (%)	97.807	96.948	96.952	95.502	97.884	96.567	97.329
		Concordance_rate (%)‡	99.701	99.550	99.551	99.686	99.640	99.845	99.695
	Het/Homo Ratio	All	1.581	1.520	1.487	1.027	1.054	1.680	1.832
		Known	1.525	1.443	1.412	0.942	1.026	1.609	1.756
		Novel	15.000	21.000	21.000	29.000	5.000	10.500	18.000
	Ti/Tv Ratio	All	3.329	2.909	2.915	3.018	3.050	2.941	2.965
		Known	3.344	2.947	2.953	3.057	3.081	2.969	2.952
		Novel	2.750	2.000	2.000	2.333	2.000	2.286	3.500
INDEL	No of variants	All	55	50	44	56	52	58	56
		Known	11	10	11	11	11	11	12
		Novel	44	40	33	45	41	47	44
		dbSNP132_rate (%)	0.200	0.200	0.250	0.196	0.212	0.190	0.214
	Het/Homo Ratio	All	1.500	0.923	0.760	0.867	0.529	1.148	1.154
		Known	0.833	0.667	0.571	0.833	0.833	0.833	2.000
		Novel	1.750	1.000	0.833	0.875	0.464	1.238	1.000

* known: dbSNP132 positions
† novel: not dbSNP132 positions
‡ concordance rate (%): the rate of the known SNPs with the same genotype as in the dbSNP132

b

		P1	P2	P3	P4	P5	P6	P7
SNV	total	15	21	21	30	12	23	18
	missense	7	9	9	14	6	12	10
	nonsense	1	0	0	1	0	0	1
	splice-5	0	1	1	0	0	0	0
	splice-3	0	0	0	0	0	0	0
	Others*	7	11	11	15	6	11	7
INDEL	total	44	40	33	45	41	47	44
	frameshift	2	4	3	3	2	4	4
	coding	3	4	4	4	2	5	4
	others†	39	32	26	38	37	38	36

* others: SNPs found in the 1000 Genome database or dbSNP131 outside the coding-region and coding-synonymous SNPs
† others: INDELs found in the 1000 Genome database or dbSNP131 or outside the coding-region

Supplementary Table 6. Summary statistics of variant analysis
(**a**) Summary Statistics of the Variants Called and PASSed Filters
(**b**) Summary Statistics of the Novel Variants Called and PASSed Filters

Nature Genetics: doi:10.1038/ng.2252

References for Supplemental Information

1. Godfrey, C. *et al.* Refining genotype phenotype correlations in muscular dystrophies with defective glycosylation of dystroglycan. *Brain : a journal of neurology* **130**, 2725-35 (2007).
2. Rodriguez-Concepcion, M. & Boronat, A. Elucidation of the methylerythritol phosphate pathway for isoprenoid biosynthesis in bacteria and plastids. A metabolic milestone achieved through genomics. *Plant physiology* **130**, 1079-89 (2002).
3. Lommel, M. *et al.* Correlation of enzyme activity and clinical phenotype in POMT1-associated dystroglycanopathies. *Neurology* **74**, 157-64 (2010).
4. Van Reeuwijk, J. *et al.* A homozygous FKRP start codon mutation is associated with Walker-Warburg syndrome, the severe end of the clinical spectrum. *Clinical genetics* **78**, 275-81 (2010).
5. Clarke, N.F. *et al.* Congenital muscular dystrophy type 1D (MDC1D) due to a large intragenic insertion/deletion, involving intron 10 of the LARGE gene. *European journal of human genetics : EJHG* **19**, 452-7 (2011).
6. Satz, J.S. *et al.* Brain and eye malformations resembling Walker-Warburg syndrome are recapitulated in mice by dystroglycan deletion in the epiblast. *The Journal of neuroscience : the official journal of the Society for Neuroscience* **28**, 10567-75 (2008).
7. Kanoff, R.J. *et al.* Walker-Warburg syndrome: neurologic features and muscle membrane structure. *Pediatric neurology* **18**, 76-80 (1998).
8. Vajsar, J., Ackerley, C., Chitayat, D. & Becker, L.E. Basal lamina abnormality in the skeletal muscle of Walker-Warburg syndrome. *Pediatric neurology* **22**, 139-43 (2000).
9. Chitayat, D. *et al.* Prenatal diagnosis of retinal nonattachment in the Walker-Warburg syndrome. *American journal of medical genetics* **56**, 351-8 (1995).

Nature Genetics: doi:10.1038/ng.2252